RGB image-based drought stress classification of garden plants using SVM model

Seong-Ju Lee
Hankyong National University
Seung-Won Han
Rural Development Administration
Tae-Wan Kim
Hankyong National University
Sung-Yung Yoo
lsn136@hknu.ac.kr

Hankyong National University

Article

Keywords: Drought stress, Garden plants, RGB image, Chlorophyll fluorescence, Support Vector Machine (SVM), Water management, Vegetation index, Precision irrigation

Posted Date: July 27th, 2025

DOI: https://doi.org/10.21203/rs.3.rs-7052665/v1

Additional Declarations: No competing interests reported.

Version of Record: A version of this preprint was published at Scientific Reports on May 7th, 2026. See the published version at https://doi.org/10.1038/s41598-026-51726-1.

Abstract

Water management in urban gardens is increasingly complex due to diverse plant species and growing drought stress under climate change. This study proposes a non-destructive method to classify drought responses of mixed garden plant species using RGB image indices and a support vector machine (SVM) model. Chlorophyll fluorescence responses were used to evaluate photosynthetic stress, while image-derived indices—green leaf index (GLI), normalized green-red difference index (NGRDI), and blue-green pigment index (BGI)—were analyzed to assess drought responses. Hierarchical clustering grouped species into three response clusters based on fluorescence and image patterns. Principal component analysis (PCA) identified NGRDI, GLI, and BGI as key variables, with NGRDI and GLI showing strong correlations with soil moisture content and BGI distinguishing cluster-specific responses. An SVM model was constructed using RGB indices and soil moisture content as input features, achieving a classification accuracy of 88.3% and an F1 score of 0.85 through five-fold cross-validation. This approach supports efficient water management and plant selection, and can be extended to precision irrigation strategies using machine learning.

Introduction

With the increasing popularity of gardening activities and lifestyles, the scope of the garden industry has expanded [1]. In response, policies have been introduced to promote garden culture and to foster the development of the associated industry through the expansion of garden infrastructure. However, the incidence of abiotic stress in plants is expected to rise with the increasing frequency of extreme weather events due to climate change [2]. Reduced precipitation with the resulting deficiency in soil moisture are emerging as the most critical environmental factors that are limiting plant growth [3]. Urban areas, in particular, are chronically dry due to impervious surfaces, such as asphalt along with high energy consumption associated with vehicles and heating systems [4]. Under such conditions, plants close their stomata to minimize water loss, which inadvertently reduces CO_2 uptake and suppresses photosynthetic activity [5]. Furthermore, managing moisture conditions in planting spaces and facilities is complicated by irregular alternating periods of floods and droughts [6]. Unlike agricultural crops that are typically grown as single species, garden plants are often cultivated as diverse species in limited spaces, which makes integrated management more complex and challenging [7]. Therefore, it is essential to identify species-specific stress responses to develop targeted management strategies with a particular emphasis on water management [8].

Under optimal growth conditions, the productivity of plants is enhanced and the efficiency of the use of light energy through photosynthesis is improved [9]. However, the photosynthetic systems of plants are severely impaired under abiotic stresses, such as excessive light, temperature extremes, water scarcity, and nutrient deficiencies [10,11]. Among these, water deficiency is considered a major environmental factor that limits photosynthetic activity [12]. It disrupts turgor pressure, restricts leaf expansion and stem elongation, and triggers stomatal closure or leaf abscission to increase water use efficiency [13]. Severe water stress inhibits photosynthesis, impairs osmotic regulation, induces major metabolic dysfunctions, and ultimately causes significant damage to plants [9]. Water stress leads to various changes in photosynthetic activity—stomatal conduction, water use efficiency, photochemical reactions, and electron transport imbalance—making it a key indicator of plant physiological status [14,15]. Chlorophyll fluorescence measurements are widely used as a non-destructive method to monitor these physiological responses [16]. For example, water stress in *Cnidium officinale* was assessed using indicators, such as the maximum quantum yield (Fv/Fm), the chlorophyll fluorescence decline ratio (Rfd_Lss), and the non-photochemical quenching at steady-state (NPQ_Lss) [17]. And according to Yoo et al. [18], the photochemical response of pepper plants was analyzed by measuring the Performance Index on an absorption basis (PI_ABS) and the Drought Factor Index (DFI) based on the OJIP method [17-19]. Furthermore, Liu, J. et al. [20] investigated the response of the photosynthetic electron transport chain in maize to varying levels of drought stress. Their findings revealed that moderate drought stress reduced the photochemical activity of PSII without affecting PSI, while severe drought stress inhibited the entire electron transport chain. The PSII was found to be more sensitive to drought stress than PSI [20].

However, due to their reliance on specialized equipment, existing non-destructive methods, such as chlorophyll fluorescence measurement, have limitations that impose spatial constraints and make field investigations challenging [21]. Hence, research using machine learning–based plant management algorithms—such as Support Vector Machine (SVM), K-nearest Neighbors (KNN), and Decision Tree (DT)—has been actively conducted with RGB (Red, Green, Blue) and hyperspectral imagery [22-27]. Approaches that evaluate plant stress by analyzing changes in light reflectance have gained increasing attention [28]. Water-stressed plants typically exhibit reduced greenness and increased reflectance in the red and blue light regions [29]. Various indices have been developed to quantitatively assess these changes. For example, the Blue-Green Pigment Index (BGI) estimates the relative concentration of pigments, such as chlorophyll and anthocyanin. The Green Leaf Index (GLI) represents the greenness of plant leaves, while the Normalized Green-Red Difference Index (NGRDI) quantifies the difference in reflectance between the green and the red spectral regions [30-32].

According to Chatterjee, S. et al. [29], the 12 RGB-based vegetation indices (VIs) obtained from Unoccupied Aerial Systems (UAS) were used to develop a machine learning regression model to predict corn yield. The optimal prediction model incorporated NGRDI, normalized green-blue difference index (NGBDI), and GLI, which were shown to play a significant role in estimating corn grain yield in isolated populations under various environmental stress conditions [29]. Additionally, Rockstad, G.B.G. et al. [22] evaluated Unmanned Aerial Vehicles (UAV)-based imagery of St. Augustine grass under both drought-stressed and well-watered conditions during turfgrass cultivation. The study confirmed that indices, such as Visible Atmospherically Resistant Index (VARI), NGRDI, and GLI, were effective to diagnose drought stress using RGB images that were similar to the results of the turfgrass field research laboratory [22].

There has been limited research that addresses the comprehensive evaluation of water response characteristics in garden environments containing diverse plant species with most existing studies focused on single species or crop-centered analyses. Therefore, our study aimed to develop a classification strategy for plant groups with similar water response characteristics using a cluster analysis of RGB image indices and chlorophyll fluorescence response data collected from 10 garden plant species. An SVM model was also employed to accurately distinguish these groups. This approach helps reduce the incidence of plant stress or damage in garden environments with mixed species, establishes a basis for systematic diagnosis of water responses, and provides foundational data to develop future precision irrigation strategies.

Materials and Methods

Drought Stress Treatment

Our study commenced on July 15, 2023 at the Hankyong National University-affiliated greenhouse (37°00’42”N, 127°19’12”E). Three replicates each of ten garden plant species, which were purchased prior to transplantation were transplanted into pots, and cultivation trials were carried out until August 30, 2023 (Table 1). The test pots measured 143 × 143 × 160 mm and were filled with silty loam as the growth medium. After transplanting the plants, the pots were placed on pallets to avoid direct contact with the ground and to minimize changes in the moisture of the soil due to ground effects. Each pot was supplied daily with a consistent amount of water through drip irrigation using Angled Drip Stake with a stabilization period of 20 days. Following stabilization, irrigation ceased to induce drought stress. During the experiment, environmental parameters inside the facility were monitored by measuring the temperature (testo 174 H, Testo Saveris GmbH, Baden-Württemberg, Germany) and soil moisture content (WaterScout SM 100, Spectrum Technologies, Inc., Aurora, IL 60504, USA) at 1-hour intervals with data logged using WatchDog 1000 Series Watermark Irrigation Stations (Spectrum Technologies Inc., Aurora, IL 60504, USA).

Table 1
List of the 10 Garden Plant Species Used in the Experiment [33]

Scientific name	**English name**	**Scientific name**	**English name**
Polygonatum odoratum	Lesser solomon's seal	*Phedimus takesimensis*	Ulleungdo stonecrop
Pachysandra terminalis	Carpet box	*Iris sanguinea*	Blood iris
Hosta plantaginea	Fragrant plantain lily	*Lilium lancifolium*	Tiger lily
Aster spathulifolius	Seashore spatulate aster	*Carex maculata*	Maculate sedge
Mukdenia rossii	Maple-leaf mukdenia	*Allium dumebuchum*	Aging chive

RGB Image Data Collection

Beginning with the transplantation date (July 15, 2023), RGB images were captured using a time-lapse camera (TLC-200, Brinno Inc., Taipei City, Taiwan). To minimize the influence of external factors on image analysis, the time-lapse camera was mounted on a pipe installed inside the greenhouse at a height of 2 meters (Fig. 1a). Each plant was photographed five times daily between 11 am and 3 pm to generate a total of 6,000 RGB images (5 shots × 3 replicates × 10 species × 40 days). The images were converted to JPG format using the 'Brinno Video Player' software (Fig. 1b).

RGB image analysis was performed using the 'FIELDimageR' package of R Studio [34] based on the method described by Matias F.I. et al. [35]. In this method, we used thresholds based on the Green Leaf Index (GLI) and Soil Color Index (SCI) to extract only the plant mask (area of interest) from the entire mask (including the background area). Pixels with a GLI value less than 0.03 were considered non-vegetated areas and removed. Areas with an SCI value greater than 0.1 were estimated as plants and plant masks (the areas of interest) were extracted. Following extraction, three band values (Blue = R_{445}, Green = R_{545}, Red = R_{650}) were obtained from the extracted plant mask (Fig. 2). The obtained band values were calculated as indices, such as BGI, GLI, and NGRDI (Table 2).

Table 2
Descriptions, formulas, and references for image indices used in the analysis

Index	**Descriptions**	**Formula**	**Related traits**
BGI [30]	Blue Green Pigment Index	B/G	Chlorophyll, LAI
GLI [31]	Green Leaf Index	(2 x G-R-B) / (2 x G + R + B)	Chlorophyll
NGRDI [32]	Normalized Green Red Difference Index	(G-R) / (G + R)	Chlorophyll, Biomass, Water content
SCI [36]	Soil Color Index	(R-G) / (R + G)	Soil Color

Chlorophyll Fluorescence Measurement

A Chlorophyll Fluorescence Meter (FP-100, Photon System Instruments, Czech Republic) in OJIP mode was used to measure chlorophyll fluorescence responses on fully expanded leaves (the third leaf from the apex) with six replicates at each of the five soil moisture levels (31.0%, 21.5%, 7.4%, 6.1%, and 4.6%). Prior to measurement, leaves were dark-adapted for 30 minutes using leaf clips to fully open PSII reaction centers and to allow energy to return to the ground state. A saturating light pulse of 3,000 μmol m^{-2} s^{-1} over a 4 mm^2 area was then applied at 80% intensity, and fluorescence was measured in OJIP mode [37].

The measured fluorescence data was used to derive chlorophyll fluorescence parameters using the JIP-Test [38]. ANOVA and Duncan's post hoc test were then performed on the basis of differences in the soil moisture content across clusters. Meanwhile, it is known that the minimum fluorescence (Fo) is measured at 50 μs when all PSII reaction centers are open, then the signal passes through the J step (2 ms) and I step (60 ms), and reaches the P step where all PSII reaction centers are closed and the maximum fluorescence (Fm) is observed [16]. Therefore, to compare the O-J-I-P response to drought stress among clusters, the measured fluorescence response was converted to ΔF and normalized (Equations 1 and 2).

$\triangle F(t) = F(t) – F(t-1)$ (1)

$\triangle F = \triangle F(t)/\triangle F_{max}$ (2)

where F(t) is the fluorescence intensity measured at time t

Data Analysis

All the data analyses in this study were performed using R Studio [34]. Hierarchical clustering analysis based on the RGB image indices and the JIP-Test parameters was performed using the ‘cluster’ package in R. The similarity between species was visualized through a dendrogram. To analyze the correlation between clusters and the drought stress characteristics, the mean value for each cluster was calculated from the RGB image indices (BGI, GLI, NGRDI) collected for each species to evaluate the drought stress response. Pearson’s correlation analysis was used to analyze the relationship between the soil moisture content and the indices. In addition, principal component analysis (PCA) was performed to distinguish between normal moisture conditions (≥ 25%) and drought stress conditions (< 25%).

SVM Model Construction

Based on the above analytical results, we developed an SVM model to classify garden plants according to their drought stress characteristics using RGB image indices. The SVM is a supervised machine learning algorithm that effectively handles both linear and nonlinear data [24]. In this study, the input variables for the SVM model included BGI, GLI, NGRDI, and soil moisture content. From the initially collected 6,000 RGB images, 1,629 high-quality samples were selected through preprocessing, which involved averaging three replicates per condition and removing outliers based on image clarity and index consistency. To address class imbalance, an additional 291 samples were generated through synthetic augmentation of minority classes, resulting in a total of 1,920 samples used for model development.

To address the class imbalance and to improve model performance, the Synthetic Minority Over-sampling Technique (SMOTE) was applied to generate new synthetic samples based on the k-nearest neighbors (k = 5) of each minority class observation. Data augmentation was conducted using the 'smotefamily' package in R with the duplicate_size parameter set to 0 to automatically balance class sizes.

The dataset was randomly divided into training (70%) and test (30%) sets. The training set was used for model development, while the test set was used to evaluate model performance. A linear kernel was employed for the SVM model, and a grid search was conducted to identify the optimal regularization parameter (C). To prevent overfitting and to assess the model’s generalization capability, 5-fold cross-validation was performed during the parameter tuning and evaluation process. Prior to training, all the input features were standardized to ensure that each variable had a comparable distribution that improved model stability and performance (Table 3).

Table 3
SVM parameter settings

Parameter	Tested value	Selected value
Kernel	Linear, Radial, Polynomial	Linear
C	0.01, 0.1, 1, 10, 100	1.0
Cross-Validation	5	5
Feature Scaling	Z-score normalization	Z-score normalization applied to all input variables (RGB indices and moisture)

We assessed model performance using multiple evaluation metrics, including Log loss, Area Under the Curve (AUC), Precision-Recall Area Under the Curve (PR AUC), Accuracy, Kappa, mean F1 score, mean sensitivity, mean specificity, mean precision, and mean balanced accuracy (Table 4) [39]. These metrics were chosen to evaluate not only the overall classification performance but also the balance between sensitivity and specificity as well as prediction accuracy. To visualize classification performance by cluster, a confusion matrix was displayed as a heatmap to identify any potential errors in classification patterns between the predicted results and the actual cluster labels.

Table 4
Model performance evaluation metrics

Measure	Formula	Evaluation focus
Accuracy	(tp + tn) / (tp + tn + fp + fn)	Overall effectiveness of a classifier
Precision	tp / (tp + fp)	Class agreement of the data labels with the positive labels given by the classifier
Recall (Sensitivity)	tp / (tp + fn)	Effectiveness of a classifier to identify positive labels
Fβ Score	$(\beta^2 + 1)tp / (\beta^2 + 1)tp + \beta^2 fn+fp$	Relation between the data’s positive labels and those assigned by a classifier
Specificity	tn / fp + tn	Effectiveness of a classifier to identify negative labels
AUC	½{[tp / (tp + fn)]+[tn / (tn + fp)]}	Classifier’s ability to avoid false classification

tp (True Positives): The number of correctly classified examples that belong to the class, tn (True Negatives): The number of correctly classified examples that do not belong to the class, fp (False Positives): The number of examples incorrectly classified as belonging to the class, fn (False Negatives): The number of examples that belong to the class but were incorrectly classified to another class, β: A parameter that adjusts the importance of recall relative to precision in the Fβ score.

Results and Discussion

Environmental Monitoring in the Greenhouse

After transplanting three replicates of ten species of garden plants, the temperature inside the greenhouse were monitored at 1-hour intervals to assess environmental conditions. The average daily temperature ranged from a minimum of 22.3°C (28 days after transplanting - DAT) to a maximum of 39.9°C (6 DAT), with an overall average of 31.6°C during the cultivation period (Fig. 3a).

Similarly, the soil moisture content was monitored hourly following transplantation. During the stabilization period (0 to 20 DAT), the average daily soil moisture content was 29.0%. When irrigation was paused, the soil moisture content decreased rapidly over time (Fig. 3b).

Hierarchical Cluster Analysis

To distinguish plant response patterns according to soil moisture content, hierarchical cluster analysis was performed using RGB image indices and chlorophyll fluorescence parameters. The BGI, GLI, and NGRDI values from the RGB images were calculated for each plant, and 16 parameters—including Fv/Fm—were derived from the chlorophyll fluorescence response using the JIP-Test. A total of 19 indices were used to generate a dendrogram to visualize species similarity and to enable their classification into three major clusters. Cluster 1 included four species (*Polygonatum odoratum, Pachysandra terminalis, Hosta plantaginea, Carex maculata*); Cluster 2 consisted of five species (*Aster spathulifolius, Phedimus takesimensis, Iris sanguinea, Lilium lancifolium, Allium dumebuchum*); and Cluster 3 comprised a single species (*Mukdenia rossii*) with distinct characteristics (Fig. 4).

Analysis of Chlorophyll Fluorescence Response

Each stage of a transition in chlorophyll fluorescence generally corresponds to specific processes at the photosystem II (PSII) reaction center: reduction of Q_A (O-J transition), reduction of reoxidation of Q_A (J-I transition), and rapid reduction of the plastoquinone (PQ) pool (I-P transition) [13,40,41]. Water deficits in plants are known to reduce photosynthetic efficiency by causing the inactivation of the photosynthetic regulatory enzyme Rubisco (ribulose-1,5-bisphosphate carboxylase/oxygenase) as well as photoinhibition damage [42]. To accurately compare temporal changes in the chlorophyll fluorescence response, the instantaneous change in fluorescence intensity (ΔF) was normalized to the total maximum change (ΔF_{max}) for the relative analysis of response differences between clusters (Fig. 5). Across all clusters, the highest fluorescence intensity during the O-J-I-P phases was observed at 31.0% soil moisture content, with fluorescence intensity significantly decreasing with the decline in moisture content. Notably, Cluster 1 exhibited the most rapid decline in ΔF during the J-I transition, which suggests severe inhibition of the Q_A^- reoxidation process in PSII. This indicates a sensitive response to drought stress at an early stage of the electron transport chain.

Therefore, the JIP-Test was conducted to analyze energy flux changes caused by drought stress (Table 5). In general, the energy flow in plants begins when chlorophyll absorbs light energy that is transferred through the antenna complex and the oxygen-evolving complex (OEC) to excite the reaction center complex. The excited reaction center releases electrons to pheophytin and reduces plastoquinone A, the primary electron acceptor. Plastoquinone A is oxidized when the electrons are transferred to plastoquinone B. When plastoquinone B accepts protons from the stroma, it is reduced to plastoquinol that then facilitates electron transport to plastocyanin through the cytochrome b6f complex and undergoes another reduction cycle. During this process, protons are pumped into the thylakoid lumen, contributing to the proton gradient required for ATP synthesis. The generated proton motive force is then used to synthesisize ATP and NADPH, which are essential for the Calvin cycle [13,43].

In our study, all clusters exhibited a significant decrease in ABS/CS (absorbed light energy per unit cross-section) and TRo/CS (excitation energy trapped by PSII reaction centers per unit cross-section) with the decrease in soil moisture content ($p < 0.001$) [44,45]. Additionally, there was a decrease in the ET2o/CS and RE1o/CS values, suggesting a reduction in the captured electron transport energy toward PSII and photosystem I (PSI), respectively, ($p < 0.001$) There was also a decline in key parameters, such as Fv/Fm (maximum quantum yield of primary PSII photochemistry) and PI_ABS (Performance index on an absorption basis), which serve as indicators of drought stress and suggest impaired functionality of the PSII. This impairment likely resulted from an inhibited electron transport and an inactivated oxygen-evolving complex (OEC), caused by a reduced reoxidation rate of Q_A^- [16,46–53]. The RC/CS (reaction center/cross section) ratio also decreased, possibly due to an increase in non-functional reaction centers. As drought stress progressed, the production of reactive oxygen species (ROS) increased due to OEC malfunction, which subsequently blocked the early steps of the electron transport chain ($p < 0.001$)

[54,55]. Inactivation of the OEC was interpreted as a disruption to the water-splitting process. This prevents the supply of electrons to the reaction centers and ultimately leads to the loss of energy capture and electron transport functionality [43]. These effects were particularly pronounced when the soil moisture content was 7.4%. Among the three clusters, Cluster 1 showed the most pronounced reduction.

Table 5 Analysis of the Effect of Soil Moisture Levels on JIP-Test Parameters Classified by Cluster. Asterisks denote statistically significant differences (DMRT): ^{ns} not significant, * $p < 0.05$, ** $p < 0.01$, *** $p < 0.001$ [38]

Cluster	Index	Soil Moisture Content				
		31.0%	21.5%	7.4%	6.1%	4.6%
Cluster 1	Fv/Fm*	0.805 ^{a}	0.751 ^{a}	0.732 ^{a}	0.598 ^{a}	0.045 ^{b}
	ABS/RC^{ns}	1.838	2.017	2.104	2.626	849.331
	RC/ABS*	0.548 ^{a}	0.514 ^{a}	0.481 ^{a}	0.42 ^{a}	0.047 ^{b}
	TRo/RC^{ns}	1.479	1.501	1.534	1.472	2.035
	DIo/RC^{ns}	0.359	0.516	0.57	1.154	847.296
	ET2o/RC^{ns}	0.848	0.935	0.858	0.623	1.957
	RE1o/RC^{ns}	0.336	0.412	0.362	0.362	-0.158
	PI_ABS**	3.064 ^{a}	3.012 ^{a}	1.771 ^{ab}	0.972 ^{b}	-0.006 ^{b}
	PI_total ABS*	1.987 ^{ab}	2.654 ^{a}	1.279 ^{ab}	0.655 ^{ab}	-0.001 ^{b}
	DF total ABS^{ns}	0.295	0.317	0.093	0.04	-4.896
	RC/CS***	19399.877 ^{a}	13417.866 ^{ab}	12058.819 ^{bc}	6174.616 ^{cd}	263.24 ^{d}
	ABS/CS***	35427.25 ^{a}	26387.067 ^{a}	24926.908 ^{ab}	14387.756 ^{bc}	4164.111 ^{c}
	TRo/CS***	28515.995 ^{a}	19781.802 ^{ab}	18274.789 ^{b}	8727.913 ^{c}	273.876 ^{c}
	ET2o/CS***	16351.962 ^{a}	12336.953 ^{ab}	10234.862 ^{b}	4269.451 ^{c}	-119.092 ^{c}
	DIo/CS^{ns}	6911.255	6605.265	6652.119	5659.842	3890.235
	RE1o/CS***	6414.394 ^{a}	5460.768 ^{a}	4313.223 ^{ab}	2167.861 ^{bc}	7.125 ^{c}
Cluster 2	Fv/Fm***	0.828 ^{a}	0.76 ^{ab}	0.701 ^{bc}	0.616 ^{cd}	0.567 ^{d}
	ABS/RC**	1.706 ^{b}	2.045 ^{ab}	2.368 ^{ab}	2.616 ^{a}	2.776 ^{a}
	RC/ABS***	0.589 ^{a}	0.493 ^{ab}	0.432 ^{b}	0.415 ^{b}	0.393 ^{b}
	TRo/RC^{ns}	1.412	1.552	1.651	1.548	1.498
	DIo/RC**	0.294 ^{c}	0.492 ^{bc}	0.717 ^{abc}	1.069 ^{ab}	1.278 ^{a}
	ET2o/RC^{ns}	0.965	1.045	1.028	0.966	0.912
	RE1o/RC***	0.357 ^{b}	0.473 ^{a}	0.449 ^{a}	0.511 ^{a}	0.529 ^{a}
	PI_ABS***	6.364 ^{a}	3.4 ^{b}	2.113 ^{b}	1.813 ^{b}	1.454 ^{b}
	PI_total ABS*	3.774 ^{a}	2.74 ^{ab}	1.635 ^{ab}	2.036 ^{ab}	2.146 ^{b}
	DF total ABS*	0.555 ^{a}	0.428 ^{a}	0.135 ^{a}	0.129 ^{a}	0.131 ^{a}
	RC/CS***	22343.366 ^{a}	13743.993 ^{b}	10239.235 ^{b}	5747.498 ^{c}	3818.848 ^{c}
	ABS/CS***	37992 ^{a}	27883.963 ^{b}	23978.8 ^{b}	13941.617 ^{c}	9709.375 ^{c}

	TRo/CS***	31463.725 ^{a}	21186.685 ^{b}	16828.969 ^{b}	8581.776 ^{c}	5574.595 ^{c}
	ET2o/CS***	21598.897 ^{a}	14328.967 ^{b}	10625.787 ^{b}	5610.952 ^{c}	3620.742 ^{c}
	DIo/CS^{ns}	6528.275	6697.278	7149.831	5359.841	4134.78
	RE1o/CS***	8015.411 ^{a}	6420.501 ^{a}	4561.135 ^{b}	2926.967 ^{bc}	2049.883 ^{c}
Cluster 3	Fv/Fm***	0.825 ^{a}	0.774 ^{ab}	0.725 ^{bc}	0.656 ^{cd}	0.59 ^{d}
	ABS/RC**	2.04 ^{c}	2.167 ^{bc}	2.402 ^{abc}	2.474 ^{ab}	2.736 ^{a}
	RC/ABS***	0.49 ^{a}	0.462 ^{ab}	0.416 ^{bc}	0.404 ^{c}	0.365 ^{c}
	TRo/RC^{ns}	1.683	1.677	1.741	1.622	1.613
	DIo/RC***	0.357 ^{c}	0.49 ^{c}	0.66 ^{bc}	0.852 ^{ab}	1.123 ^{a}
	ET2o/RC***	0.89 ^{b}	0.968 ^{a}	0.888 ^{bc}	0.811 ^{c}	0.828 ^{bc}
	RE1o/RC^{ns}	0.409	0.537	0.474	0.485	0.509
	PI_ABS***	2.593 ^{a}	2.159 ^{a}	1.143 ^{b}	0.77 ^{bc}	0.554 ^{c}
	PI_total ABS***	2.205 ^{a}	2.685 ^{a}	1.306 ^{b}	1.147 ^{b}	0.882 ^{b}
	DF total ABS***	0.343 ^{a}	0.429 ^{a}	0.116 ^{b}	0.059 ^{b}	-0.054 ^{b}
	RC/CS***	21083.539 ^{a}	15607.223 ^{b}	12438.747 ^{c}	8337.357 ^{d}	6101.624 ^{d}
	ABS/CS***	43004.25 ^{a}	33816.667 ^{b}	29872.833 ^{b}	20623.5 ^{c}	16694.333 ^{c}
	TRo/CS***	35478.506 ^{a}	26174.1 ^{b}	21657.804 ^{b}	13522.142 ^{c}	9844.092 ^{c}
	ET2o/CS***	18759.26 ^{a}	15111.18 ^{b}	11045.48 ^{c}	6763.324 ^{d}	5053.301 ^{d}
	DIo/CS^{ns}	7525.744	7642.567	8215.029	7101.359	6850.241
	RE1o/CS***	8621.277 ^{a}	8375.712 ^{a}	5890.923 ^{b}	4045.374 ^{c}	3104.17 ^{c}

Fv/Fm: Maximum quantum yield of primary PSII photochemistry, ABS/RC: Absorption flux per RC, RC/ABS: Number of Q_A reducing RCs per PSII antenna Chl, TRo/RC: Trapped energy flux per RC (at t = 0), DIo/RC: Dissipated energy flux per RC (at t = 0), ET2o/RC: Electron transport flux from Q_A to Q_B per RC (at t = 0), RE1o/RC: Electron transport flux until PSI acceptors per RC (at t = 0), PI_ABS: Performance index for energy conservation from photons absorbed by PSII antenna to the reduction of Q_B, PI_total ABS: Performance index for energy conservation from photons absorbed by PSII antenna, until the reduction of PSI acceptors, DF total ABS: Driving force on absorption basis, RC/CS: Density of RCs (Q_A-reducing PSII reaction centers), ABS/CS: Absorption flux per CS 'x' can be 'Chl', 0 or 'M', TRo/CS: Trapped energy flux per CS (at t = 0), ET2o/CS: Electron transport flux per CS (at t = 0), DIo/CS: Dissipated energy flux per CS (at t = 0), RE1o/CS: Electron transport flux until PSI acceptors per CS (at t = 0).

RGB Image Analysis

In general, healthy plant leaves are known to reflect green (G) and near-infrared (NIR) light, while absorbing blue (B) and red (R) light [29]. Based on these optical properties, higher vegetation index values are associated with better plant growth and health status [22,23,30]. In our study, we observed a decrease in both GLI and NGRDI across all clusters as the soil dried with a particularly sharp decline when soil moisture content dropped below 10% (Fig. 6a, 6b). Correlation analysis further confirmed that GLI and NGRDI were significantly correlated with soil moisture content in all the clusters ($p < 0.001$) (Fig. 7). Notably, NGRDI exhibited the strongest correlation ($r > 0.9$) with soil moisture. This was consistent with previous findings suggesting that NGRDI is one of the most efficient indicators to estimate crop water use efficiency (WUE) among various vegetation indices [22,29,56]. In contrast, BGI did not show a consistent trend with changes in soil moisture content, and its correlation with moisture was not statistically significant in most clusters (Fig. 6c, Fig. 7).

Water-stressed plants exhibit reduced chlorophyll concentration, leading to decreased light absorption and alterations in spectral reflectance patterns [57,58]. In particular, water deficit causes a decline in total chlorophyll and chlorophyll a content, both of which are strongly associated with absorption in the red wavelength region. Red light absorption tends to decrease as chlorophyll degrades or photosynthetic capacity declines, while red reflectance increases [59]. Consequently, red reflectance has been widely used as a key indicator to evaluate plant water stress. The vegetation indices analyzed in this study—GLI and NGRDI—are also derived using red wavelength information [60–62]. Therefore, they can serve as effective indicators to detect water stress in plants. In contrast, the blue wavelength is primarily absorbed by chlorophyll b. The changes in blue reflectance under water stress conditions are generally less pronounced than those observed in the red region [63]. There was limited sensitivity of BGI, which is based on blue reflectance, to water stress in our study. This was interpreted as minimal direct correlation of BGI with drought response.

Establishment of an SVM model to classify drought stress characteristics of garden plants

To investigate the correlation of drought stress characteristics of different clusters, principal component analysis (PCA) was conducted for six different soil moisture conditions. These conditions were categorized into normal moisture (≥ 25%) and drought stress (< 25%) groups, based on the analysis of chlorophyll fluorescence response and RGB image indices.

Principal component 1 (PC1) accounted for 67.7% of the total variance and exhibited high negative loadings with soil moisture content (-0.544), GLI (-0.587), and NGRDI (-0.572). Principal component 2 (PC2) explained an additional 27.5% of the variance and showed a strong positive loading with BGI (0.907). Together, PC1 and PC2 explained 95.2% of the total variance and highlighted the primary axes of variation. These results indicate that soil moisture, GLI, NGRDI, and BGI significantly contribute to distinguish drought stress characteristics among clusters (Table 6). In the distribution of garden plant clusters by soil moisture content, drought-stressed (right side) and well-watered plants (left side) were clearly separated along PC1. This confirms that GLI and NGRDI are effective indicators to diagnose drought stress. Meanwhile, PC2 revealed inter-cluster differences. This suggests that BGI may be useful to differentiate between clusters (Fig. 8).

Table 6
Loadings of Variables on Principal Components 1 and 2 in PCA Analysis

PC1				PC2			
Index	**Positive**	**Index**	**Negative**	**Index**	**Positive**	**Index**	**Negative**
BGI	0.181	GLI	-0.587	BGI	0.907	GLI	-0.209
		NGRDI	-0.572	Moisture	0.277		
		Moisture	-0.544	NGRDI	0.238		

The PCA results were utilized to classify the clusters by constructing an SVM model. The SVM model, developed using RGB image indices (GLI, NGRDI, and BGI), achieved an accuracy of 88.3% and an F1 score of 0.85 through cross-validation (Table 7). The confusion matrix visualized as a heatmap clearly distinguished the clusters (Fig. 9). These results indicate that the SVM model was effective to classify drought stress characteristics of garden plants, suggesting that RGB image data can serve as a valuable metric to classify stress.

Table 7
5-Fold Cross-Validation Performance Metrics of the SVM Model

Metric	5-Fold CV Mean	Metric	5-Fold CV Mean
Log Loss	0.301	F1 Score	0.849
AUC (Area Under the Curve)	0.966	Sensitivity	0.843
PR AUC (Precision-Recall AUC)	0.906	Specificity	0.942
Accuracy	0.883	Precision	0.858
Kappa	0.812	Balanced Accuracy	0.892

Conclusions

Our study presents a method to effectively classify diverse garden plant species based on their drought stress response characteristics. Using 10 species commonly co-planted in urban gardens, we integrated RGB image indices and chlorophyll fluorescence response data and developed a machine learning-based Support Vector Machine (SVM) model. Our data analysis revealed that the photosynthetic efficiency was reduced when drought stress inhibited the Q_A^- reoxidation process in PSII, disrupted electron transport, deactivated the oxygen-evolving complex (OEC), and increased red light reflectance.

Plants were grouped, using hierarchical clustering, into three clusters based on their drought response. Principal component analysis (PCA) helped to identify major sources of variation. The GLI and the NGRDI exhibited strong positive correlations with soil moisture content and served as reliable indicators of plant water status and growth conditions. The BGI was useful to distinguish subtle inter-cluster differences. The SVM model, trained using GLI, NGRDI, BGI, and soil moisture content, achieved high classification performance with 88.3% accuracy and an F1 score of 0.85 through five-fold cross-validation.

These findings suggest that drought stress responses in complex planting environments can be effectively classified by integrating non-destructive image analysis with machine learning. However, its application in diverse field conditions may be constrained as our study was limited to just 10 species in a controlled greenhouse setting. We also did not take into full consideration the temporal dynamics of stress and recovery. Hence, RGB-based indices may be limited in accurately capturing physiological changes.

Future studies should involve repeated trials in open-field environments, include diverse vegetation types, and enhance the quality of the models using multispectral or hyperspectral data. When such efforts are integrated with advanced machine learning algorithms, they have the potential to contribute to the development of precision irrigation strategies and adaptive planting management systems.

Declarations

Data availability

The datasets are provided within the manuscript or supplementary information files.

Acknowledgements

The authors appreciate the financial support provided by the National Institute of Horticultural and Herbal Science (RS-2021-RD009681), Rural Development Administration, Republic of Korea.

Author contributions

S.J. conceptualized the study, developed the methodology, implemented the software, performed the investigation, curated the data, visualized the results, and wrote the original draft. S.J., S.W., and S.Y. validated the data. S.W. and S.Y. reviewed and edited the manuscript. S.Y. and T.W. supervised the project and provided critical feedback. S.Y. administered the project and acquired the funding. All authors read and approved the final version of the manuscript.

Funding

This work was supported by a grant (Project NO. RS-2021-RD009681) from RDA (Rural Development Administration), Republic of Korea.

Competing interests

The authors declare no competing interests.

Additional information

Correspondence and requests for materials should be addressed to S.Y. or T.W.

References

1. in *Korea Forest Service* 2-9 (2021).
2. Fedoroff, N. V. *et al.* Radically Rethinking Agriculture for the 21st Century. *Science* **327**, 833-834, doi:10.1126/science.1186834 (2010).
3. Araus, J. L. Plant Breeding and Drought in C3 Cereals: What Should We Breed For? *Annals of Botany* **89**, 925-940, doi:10.1093/aob/mcf049 (2002).
4. Kim, J. S., Jung, M. I., Han, S. W. & Jang, H. K. in *Society for People, Plants, and Environment.* 39-39.
5. Bae, H. H. *et al.* Physiological and Proteome Responses of Korean F1 maize (Zea mays L.) Hybrids to Water-deficit Stress during Tassel Initiation. *Korean J. Crop Sci.* **64**, 422-431, doi:10.7740/kjcs.2019.64.4.422 (2019).
6. Park, J. Y., Yoo, J. Y., Lee, M. & Kim, T.-W. Assessment of Drought Risk in Korea: Focused on Data-based Drought Risk Map. *Journal of The Korean Society of Civil Engineers* **32**, 203-211, doi:10.12652/ksce.2012.32.4b.203 (2012).
7. Adams, C. R. (Routledge, 2012).
8. Shinozaki, K. & Yamaguchi-Shinozaki, K. Gene networks involved in drought stress response and tolerance. *Journal of Experimental Botany* **58**, 221-227, doi:10.1093/jxb/erl164 (2006).
9. Taiz, L., Møller, I. M., Murphy, A. & Zeiger, E. (Oxford University Press, 2023).
10. Pereira, A. Plant Abiotic Stress Challenges from the Changing Environment. *Frontiers in Plant Science* **7**, doi:10.3389/fpls.2016.01123 (2016).
11. Zhu, J.-K. Abiotic Stress Signaling and Responses in Plants. *Cell* **167**, 313-324, doi:10.1016/j.cell.2016.08.029 (2016).

12. Kim, K. S. *et al.* Effect of Soil Water and Shading Treatment on Chlorophyll Fluorescence Parameters and Photosynthetic Capacity in Cnidium officinale Makino. *Korean Journal of Medicinal Crop Science* **28**, 412-420, doi:10.7783/kjmcs.2020.28.6.412 (2020).
13. Lee, K. C., Kim, S. H., Park, W. G. & Kim, Y. S. Effects of Drought Stress on Photosynthetic Capacity and Photosystem II Activity in Oplopanax elatus. *Korean Journal of Medicinal Crop Science* **22**, 38-45, doi:10.7783/kjmcs.2014.22.1.38 (2014).
14. Sun, Y., Wang, C., Chen, H. Y. H. & Ruan, H. Response of Plants to Water Stress: A Meta-Analysis. *Frontiers in Plant Science* **11**, doi:10.3389/fpls.2020.00978 (2020).
15. Wu, J. *et al.* Physiology of Plant Responses to Water Stress and Related Genes: A Review. *Forests* **13**, 324, doi:10.3390/f13020324 (2022).
16. Strasser, R. J., Srivastava, A. & Tsimilli-Michael, M. The fluorescence transient as a tool to characterize and screen photosynthetic samples. *Probing photosynthesis: mechanisms, regulation and adaptation*, 445-483 (2000).
17. Kim, K. S. *et al.* Effect of Soil Water and Shading Treatment on Chlorophyll Fluorescence Parameters and Photosynthetic Capacity in Cnidium officinale Makino. *The Korean Society of Medicinal Crop Science* **28**, 412-420, doi:10.7783/KJMCS.2020.28.6.412 (2020).
18. Yoo, S.-Y. *et al.* Photochemical Response Analysis on Drought Stress for Red Pepper (Capsiumannuum L.). *Korean Journal of Soil Science and Fertilizer* **46**, 659-664, doi:10.7745/kjssf.2013.46.6.659 (2013).
19. Oukarroum, A., Madidi, S. E., Schansker, G. & Strasser, R. J. Probing the responses of barley cultivars (Hordeum vulgare L.) by chlorophyll a fluorescence OLKJIP under drought stress and re-watering. *Environmental and Experimental Botany* **60**, 438-446, doi:10.1016/j.envexpbot.2007.01.002 (2007).
20. Liu, J. *et al.* Effects of Drought Stress on the Photosynthesis in Maize. *Russian Journal of Plant Physiology* **65**, 849-856, doi:10.1134/s1021443718060092 (2018).
21. Kim, N.-S., Lee, H.-C. & Cha, J.-Y. A Study on Changes of Phenology and Characteristics of Spatial Distribution Using MODIS Images. *Journal of the Korea Society of Environmental Restoration Technology* **16**, 59-69, doi:10.13087/kosert.2013.16.5.059 (2013).
22. Rockstad, G. B. G., Austin, R. E., Gouveia, B. T., Carbajal, E. M. & Milla-Lewis, S. R. Assessing unmanned aerial vehicle-based imagery for breeding applications in St. Augustinegrass under drought and non-drought conditions. *Crop Science* **64**, 496-510, doi:10.1002/csc2.21128 (2023).
23. Lóránt, B., Veronika, K.-B. & József, B. Comparison of RGB Indices used for Vegetation Studies based on Structured Similarity Index (SSIM). *Journal of Plant Science and Phytopathology* **8**, 007-012, doi:10.29328/journal.jpsp.1001124 (2024).
24. Song, H.-Y., Cho, B.-H., Kim, Y.-H. & Kim, K.-C. Development of a classification model for tomato maturity using hyperspectral imagery. *Korean Journal of Agricultural Science* **49**, 129-136, doi:10.7744/kjoas.20220010 (2022).
25. Feng, H., Tao, H., Li, Z., Yang, G. & Zhao, C. Comparison of UAV RGB Imagery and Hyperspectral Remote-Sensing Data for Monitoring Winter Wheat Growth. *Remote Sensing* **14**, 3811, doi:10.3390/rs14153811 (2022).
26. Starý, K., Jelínek, Z., Kumhálová, J., Chyba, J. & Balážová, K. Comparing RGB-based vegetation indices from UAV imageries to estimate hops canopy area. doi:10.15159/ar.20.169 (2020).
27. do Amaral, E. S. *et al.* Relationships between reflectance and absorbance chlorophyll indices with RGB (Red, Green, Blue) image components in seedlings of tropical tree species at nursery stage. *New Forests* **50**, 377-388, doi:10.1007/s11056-018-9662-4 (2018).
28. Berger, K. *et al.* Crop nitrogen monitoring: Recent progress and principal developments in the context of imaging spectroscopy missions. *Remote Sensing of Environment* **242**, 111758, doi:10.1016/j.rse.2020.111758 (2020).
29. Chatterjee, S., Adak, A., Wilde, S., Nakasagga, S. & Murray, S. C. Cumulative temporal vegetation indices from unoccupied aerial systems allow maize (Zea mays L.) hybrid yield to be estimated across environments with fewer flights. *Plos one* **18**, e0277804 (2023).

30. Zarcotejada, P. *et al.* Assessing vineyard condition with hyperspectral indices: Leaf and canopy reflectance simulation in a row-structured discontinuous canopy. *Remote Sensing of Environment* **99**, 271-287, doi:10.1016/j.rse.2005.09.002 (2005).
31. Louhaichi, M., Borman, M. M. & Johnson, D. E. Spatially Located Platform and Aerial Photography for Documentation of Grazing Impacts on Wheat. *Geocarto International* **16**, 65-70, doi:10.1080/10106040108542184 (2001).
32. Tucker, C. J. Red and photographic infrared linear combinations for monitoring vegetation. *Remote Sensing of Environment* **8**, 127-150, doi:10.1016/0034-4257(79)90013-0 (1979).
33. Korea Forest Service, K. N. A. *Nature*, <http://www.nature.go.kr/main/Main.do> (1998).
34. R : A language and environment for statistical computing v. 4.1.2 (2021).
35. Matias, F. I., Caraza-Harter, M. V. & Endelman, J. B. FIELDimageR: An R package to analyze orthomosaic images from agricultural field trials. *The Plant Phenome Journal* **3**, doi:10.1002/ppj2.20005 (2020).
36. Mathieu, R., Pouget, M., Cervelle, B. & Escadafal, R. Relationships between satellite-based radiometric indices simulated using laboratory reflectance data and typic soil color of an arid environment. *Remote sensing of environment* **66**, 17-28 (1998).
37. Ayyaz, A. *et al.* Melatonin induced changes in photosynthetic efficiency as probed by OJIP associated with improved chromium stress tolerance in canola (Brassica napus L.). *Heliyon* **6**, e04364, doi:10.1016/j.heliyon.2020.e04364 (2020).
38. Stirbet, A. & Govindjee. On the relation between the Kautsky effect (chlorophyll a fluorescence induction) and Photosystem II: Basics and applications of the OJIP fluorescence transient. *Journal of Photochemistry and Photobiology B: Biology* **104**, 236-257, doi:10.1016/j.jphotobiol.2010.12.010 (2011).
39. Sokolova, M. & Lapalme, G. A systematic analysis of performance measures for classification tasks. *Information Processing & Management* **45**, 427-437, doi:10.1016/j.ipm.2009.03.002 (2009).
40. Stirbet, A., Govindjee, Strasser, B. J. & Strasser, R. J. ChlorophyllaFluorescence Induction in Higher Plants: Modelling and Numerical Simulation. *Journal of Theoretical Biology* **193**, 131-151, doi:10.1006/jtbi.1998.0692 (1998).
41. Oh, S.-J., Zhin, K.-L. & Koh, S.-C. Characterization of Chl a Fluorescence of Hydrophytes under Cadmium Stress. *Journal of Environmental Science International* **18**, 1361-1368, doi:10.5322/jes.2009.18.12.1361 (2009).
42. Yoo, S.-Y., Eom, K.-C., Park, S.-H. & Kim, T.-W. Possibility of Drought stress Indexing by Chlorophyll Fluorescence Imaging Technique in Red Pepper (Capsicum annuum L.). *Korean Journal of Soil Science and Fertilizer* **45**, 676-682, doi:10.7745/kjssf.2012.45.5.676 (2012).
43. Kim Jin-Seog, C. K. M., Park Kee Woong. Action Physiology and Characteristics of Various Chemicals Inducing Bleaching(Whitening) of Higher Plants. *Weed&Turfgrass Science* **13**, 31-51, doi:10.5660/WTS.2024.13.1.3 (2024).
44. Oh, S. & Koh, S. C. Chlorophyll a Fluorescence Response to Mercury Stress in the Freshwater Microalga Chlorella Vulgaris. *Journal of Environmental Science International* **22**, 705-715, doi:10.5322/jesi.2013.22.6.705 (2013).
45. Shin, Y. K. *Evaluation of abiotic stress tolerance in vegetable plug seedlings using non-destructive chlorophyll fluorescence analysis*, Jeonbuk National University Graduate School, (2022).
46. Strasser, R. J., Tsimilli-Michael, M. & Srivastava, A. in *Advances in Photosynthesis and Respiration* 321-362 (Springer Netherlands, 2004).
47. Rathod, D. P. Chlorophyll a fluorescence determines the drought resistance capabilities in two varieties of mycorrhized and non-mycorrhized Glycine max Linn. *African Journal of Microbiology Research* **5**, doi:10.5897/ajmr11.737 (2011).
48. Govindjee, Downton, W. J. S., Fork, D. C. & Armond, P. A. Chlorophyll A fluorescence transient as an indicator of water potential of leaves. *Plant Science Letters* **20**, 191-194, doi:10.1016/0304-4211(81)90261-3 (1981).
49. Havaux, M. & Lannoye, R. Chlorophyll fluorescence induction: A sensitive indicator of water stress in maize plants. *Irrigation Science* **4**, 147-151, doi:10.1007/bf00273382 (1983).
50. Ögren, E. Evaluation of Chlorophyll Fluorescence as a Probe for Drought Stress in Willow Leaves. *Plant Physiology* **93**, 1280-1285, doi:10.1104/pp.93.4.1280 (1990).

51. van Rensburg, L., Krüger, G. H. J., Eggenberg, P. & Strasser, R. J. Can screening criteria for drought resistance in Nicotiana tabacum L. be derived from the polyphasic rise of the chlorophyll a fluorescence transient (OJIP)? *South African Journal of Botany* **62**, 337-341, doi:10.1016/s0254-6299(15)30676-1 (1996).
52. Lu, C. Effects of water stress on photosystem II photochemistry and its thermostability in wheat plants. *Journal of Experimental Botany* **50**, 1199-1206, doi:10.1093/jexbot/50.336.1199 (1999).
53. Rolando, C. A. & Little, K. M. Using chlorophyll fluorescence to determine stress in *Eucalyptus grandis* seedlings. *The Southern African Forestry Journal* **197**, 5-12, doi:10.1080/20702620.2003.10431716 (2003).
54. Lidon, F. C. & Henriques, F. S. Oxygen metabolism in higher plant chloroplasts. *Photosynthetica* **29**, 249–279 (1993).
55. Asada, K. THE WATER-WATER CYCLE IN CHLOROPLASTS: Scavenging of Active Oxygens and Dissipation of Excess Photons. *Annual Review of Plant Physiology and Plant Molecular Biology* **50**, 601-639, doi:10.1146/annurev.arplant.50.1.601 (1999).
56. Yang, M. *et al.* Assessment of Water and Nitrogen Use Efficiencies Through UAV-Based Multispectral Phenotyping in Winter Wheat. *Frontiers in Plant Science* **11**, doi:10.3389/fpls.2020.00927 (2020).
57. Zarco-Tejada, P. Chlorophyll Fluorescence Effects on Vegetation Apparent Reflectance I. Leaf-Level Measurements and Model Simulation. *Remote Sensing of Environment* **74**, 582-595, doi:10.1016/s0034-4257(00)00148-6 (2000).
58. Murtha, P. A. in *Remote Sensing in Resource Management. Soil Conser. Soc. Amer., Ankeny, IA.* 141-158.
59. Govender, M., Govender, P. J., Weiersbye, I. M., Witkowski, E. T. F. & Ahmed, F. Review of commonly used remote sensing and ground-based technologies to measure plant water stress. *Water SA* **35**, doi:10.4314/wsa.v35i5.49201 (2009).
60. Blackburn, G. A. Hyperspectral remote sensing of plant pigments. *Journal of Experimental Botany* **58**, 855-867, doi:10.1093/jxb/erl123 (2006).
61. Blackburn, G. A. Relationships between Spectral Reflectance and Pigment Concentrations in Stacks of Deciduous Broadleaves. *Remote Sensing of Environment* **70**, 224-237, doi:10.1016/s0034-4257(99)00048-6 (1999).
62. Curran, P. J., Dungan, J. L. & Gholz, H. L. Exploring the relationship between reflectance red edge and chlorophyll content in slash pine. *Tree Physiology* **7**, 33-48, doi:10.1093/treephys/7.1-2-3-4.33 (1990).
63. GUYOT, G. & BARET, F. in *Proc. 4th Int. Symp. Spectral Signatures of Objects in Remote Sens.* 18-22.

Figures

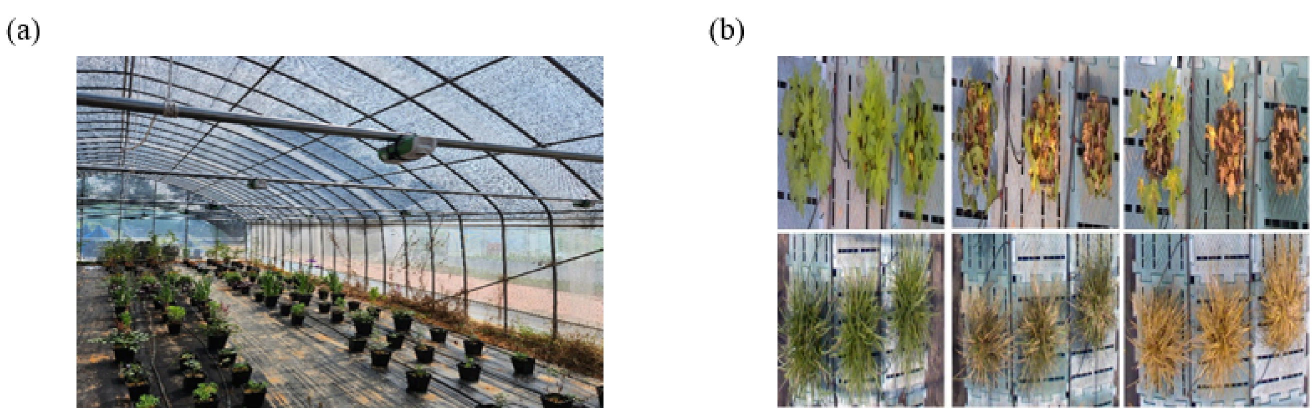

Figure 1

Field setup and collection of RGB images: (a) Field plot layout, (b) Examples of RGB images captured by a time-lapse camera

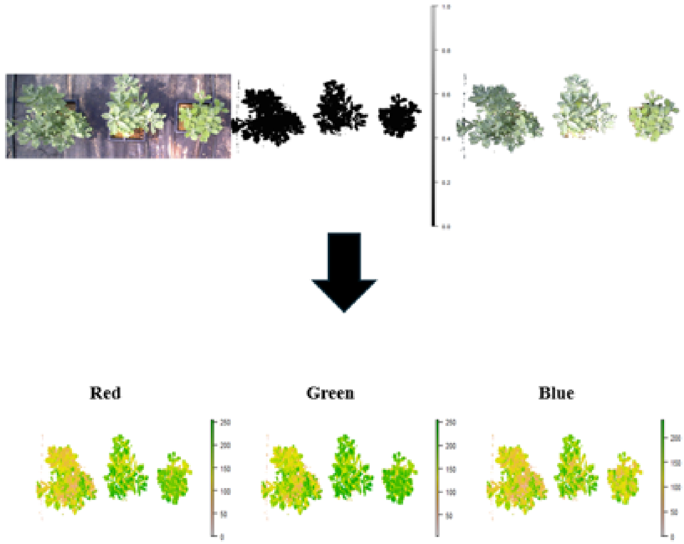

Figure 2

Extraction of plant mask from RGB images: Isolation of the plant mask (area of interest) from the total mask (including the background area) and retrieval of the band values (Blue = R_{445}, Green = R_{545}, Red = R_{650})

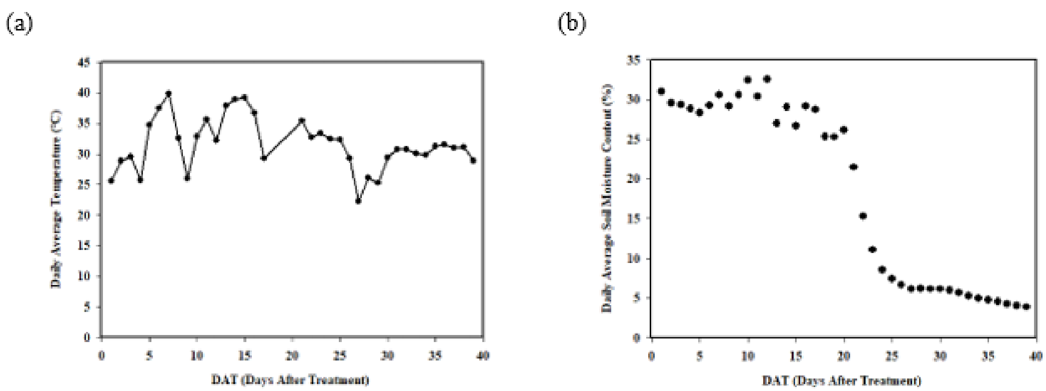

Figure 3

Microclimatic conditions and soil moisture content in the greenhouse after transplantation: (a) Daily average temperature (°C), (b) Daily average soil moisture content (%)

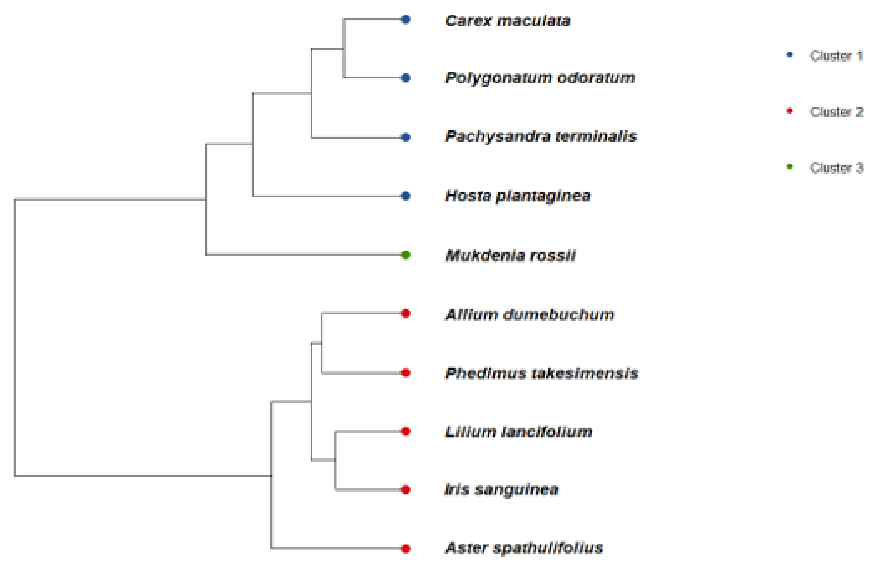

Figure 4

Dendrogram illustrating the clustering of plant species based on BGI, GLI, NGRDI Values and chlorophyll fluorescence parameters

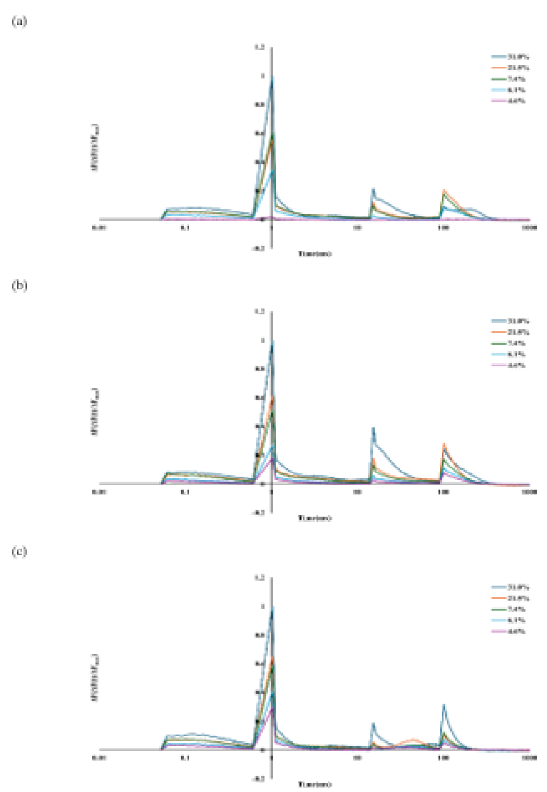

Figure 5

Comparison of Chlorophyll Fluorescence Response Across Soil Moisture Conditions by Cluster: (**a**) Cluster 1, (**b**) Cluster 2, and (**c**) Cluster 3

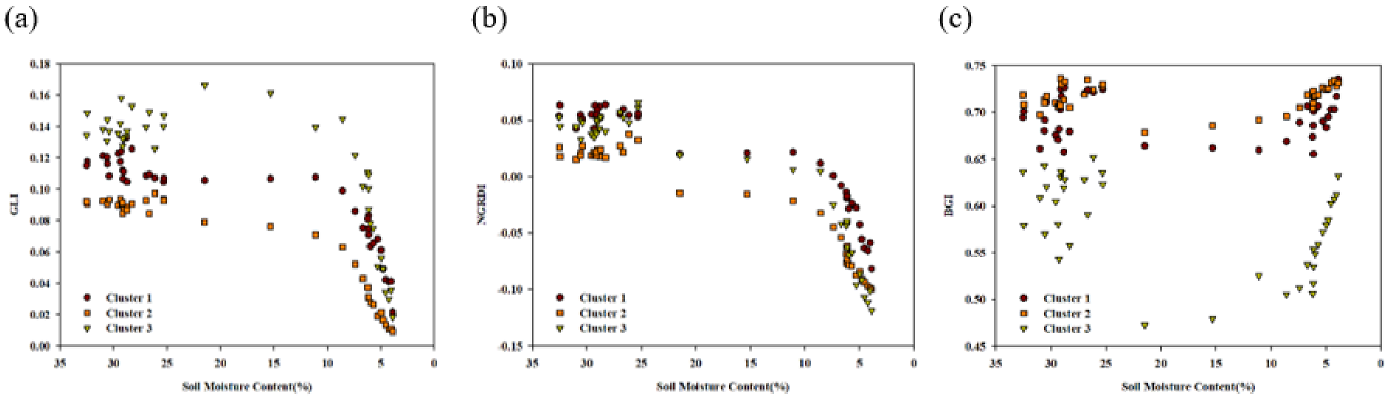

Figure 6

Changes in RGB Image Indices Across Clusters in Response to Soil Moisture Content: (a) GLI, (b) NGRDI, (c) BGI

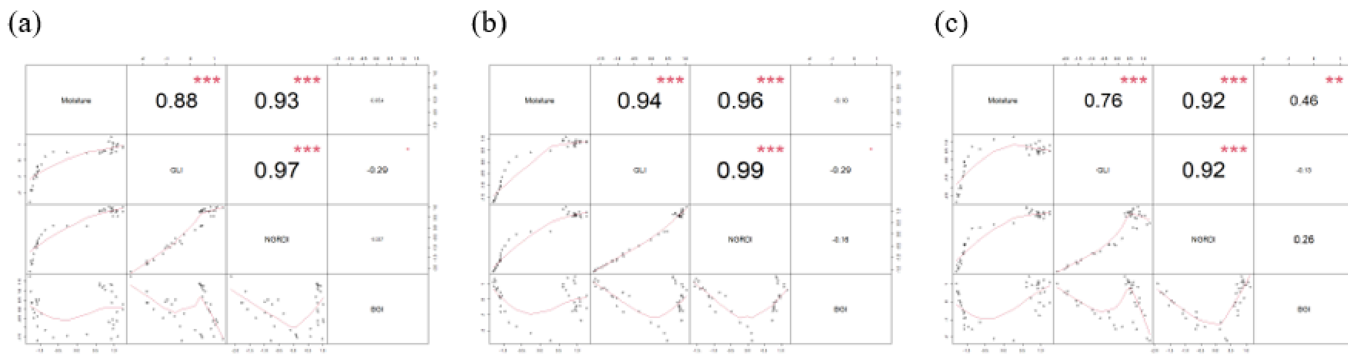

Figure 7

Pearson Correlation Analysis Between Soil Moisture Content and RGB Image Indices Across Clusters: (a) Cluster 1, (b) Cluster 2, (c) Cluster 3. Asterisks denote statistically significant differences: * $p < 0.05$, ** $p < 0.01$, *** $p < 0.001$

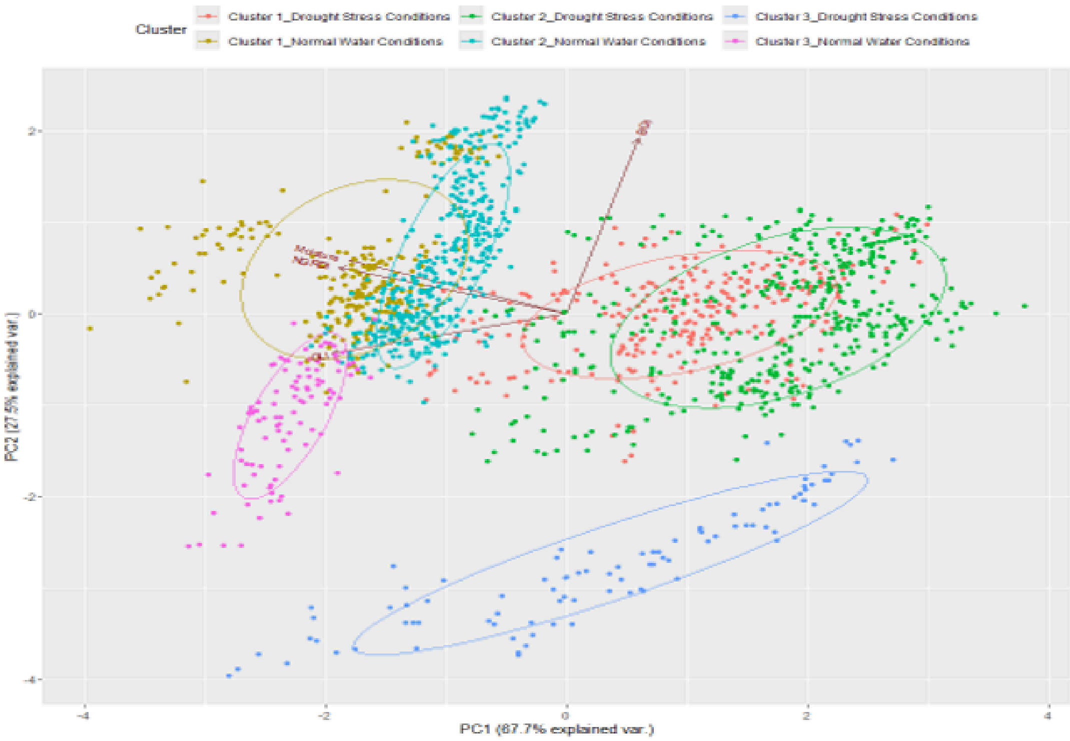

Figure 8

Principal Component Analysis (PCA) of Plant Response To Drought and Normal Water Conditions Across Clusters

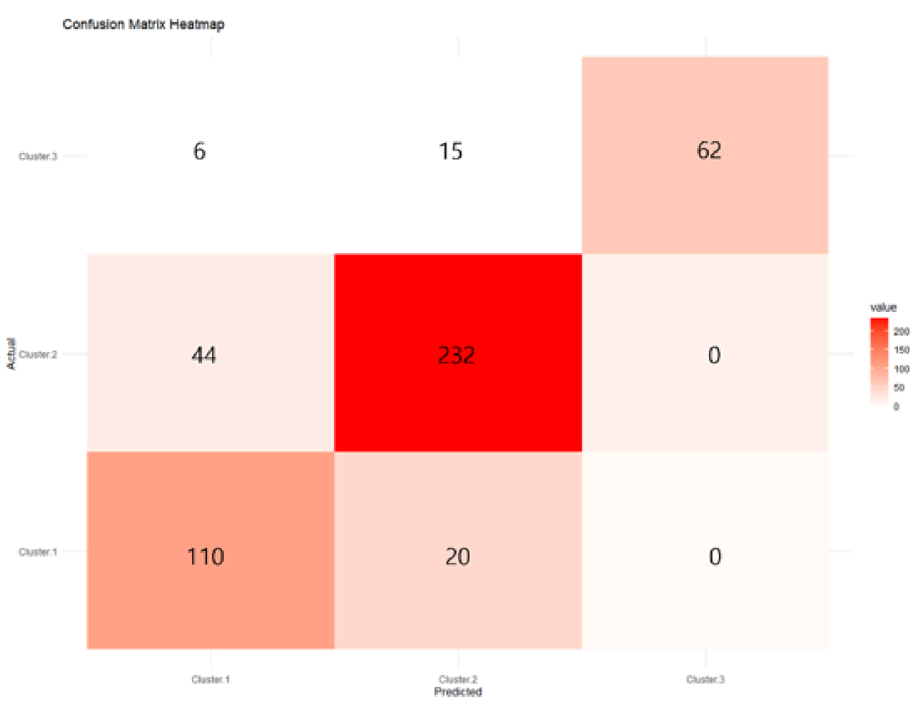

Figure 9

Confusion Matrix Visualization of SVM Model Performance

Supplementary Files

This is a list of supplementary files associated with this preprint. Click to download.

- SupplementarymaterialRGBimagebaseddroughtstressclassificationofgardenplantsusingSVMmodelScientificReports.xlsx